JOC The Journal of Organic Chemistry

Article

pubs.acs.org/joc

# Tuning the Rotation Rate of Light-Driven Molecular Motors

Jurica Bauer, Lili Hou, Jos C. M. Kistemaker, and Ben L. Feringa*

Centre for Systems Chemistry, Stratingh Institute for Chemistry, and Zernike Institute for Advanced Materials, Faculty of Mathematics and Natural Sciences, University of Groningen, Nijenborgh 4, 9747 AG Groningen, The Netherlands

Supporting Information

**ABSTRACT:** Overcrowded alkenes are among the most promising artificial molecular motors because of their ability to undergo repetitive light-driven unidirectional rotary motion around the central C═C bond. The exceptional features of these molecules render them highly useful for a number of applications in nanotechnology. Many of these applications, however, would benefit from higher rotation rates. To this end, a new molecular motor was designed, and the isomerization processes were studied in detail. The new motor comprises a fluorene lower half and a five-membered-ring upper half; the upper-half ring is fused to a *p*-xylyl moiety and bears a *tert*-butyl group at the stereogenic center. The kinetics of the thermal isomerization was studied by low-temperature UV−vis spectroscopy as well as by transient absorption spectroscopy at room temperature. These studies revealed that the *tert*-butyl and *p*-xylyl groups in the five-membered-ring upper half may be introduced simultaneously in the molecular design to achieve an acceleration of the rotation rate of the molecular motor that is larger than the acceleration obtained by using either one of the two groups individually. Furthermore, the new molecular motor retains unidirectional rotation while showing remarkably high photostationary states.

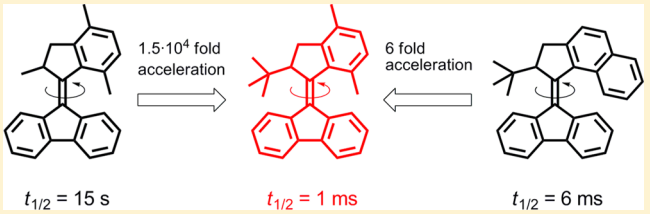


## INTRODUCTION

Many naturally occurring processes involve nanometer-scale molecular motors.[1] Myosins are a family of motor proteins that act in concert to achieve muscle contraction. Kinesins and dyneins are present in eukaryotic cells, where they transport cellular cargo along the microtubule filaments. The bacterial flagellar motor is responsible for the movement of numerous cellular organisms, while the $F_1$ motor of ATP synthase drives the synthesis of ATP in cells. These are but a few examples of the frequent occurrence of molecular motors in essential biological processes. All of them share a common goal, however, and that is to harness work.[1]

The prospect of future nanotechnology has stimulated great interest in the development of artificial molecular motors taking inspiration from nature in providing work at the molecular level. Such molecular motors could undoubtedly play a fundamental role in the development of future dynamic molecular systems, nanodevices, and machines.[2−4] Intrinsic to these systems is the conversion of energy into controlled motion. Several entirely synthetic molecular motors have been designed to provide controlled linear or rotary motion by making use of chemical energy, light energy, or electron-transfer processes.[2−15] Furthermore, recent developments have allowed work to be harnessed from both synthetic linear molecular motors[16] and rotary molecular motors.[17,18]

Overcrowded alkenes are among the most promising classes of artificial molecular motors because of their ability to undergo repetitive light-driven unidirectional rotary motion around the central C═C bond (the rotary axle). The rotation occurs through two fast photochemical isomerization steps and two slow and rate-determining thermal helix-inversion steps.[19] These synthetic molecules have been shown to perform work not only at the molecular level[18] but at the microscopic level as well.[17]

The ability to tune the rotation rate is of utmost importance for the development of new and more complex motor systems as well as for their ultimate application in molecular machines.[20−22] Working with a slower motor may be desirable when trying to introduce new concepts, as the isomerization processes are often easier to follow and the changes in properties are more readily studied with a slower motor than with a fast one.[23] However, application will most often favor faster motors, as higher rotation rates of the motor will compete better with the "Brownian storm" of molecular vibrations and collisions.[2−4,20,21] Furthermore, it is highly desirable to have a system with a short response time. Yet another advantage of a faster-rotating molecular motor is that it will deliver more work per unit time than a slow one (provided that they both deliver the same work per rotation). In a rotational system, the power $P$ is (classically) expressed[24] as the scalar product of the torque, $\boldsymbol{\tau}$, and the angular velocity, $\boldsymbol{\omega}$; $P = \boldsymbol{\tau}\cdot\boldsymbol{\omega}$. This means that a faster-rotating motor will have higher power!

Our group has designed, prepared, and studied a number of molecular rotary motors.[5] Investigating the rate of rotation has always been paramount to their characterization as molecular motors.[20,21,25] During the course of this research, it has been shown that the structures of both the upper and lower halves of the motor have a strong influence on the rotation rate. Many

**Received:** February 20, 2014
**Published:** April 15, 2014

   dx.doi.org/10.1021/jo500411z | J. Org. Chem. 2014, 79, 4446−4455

interesting structure−rate trends have arisen (Scheme 1). For example, employing a five-membered ring in the upper half of

**Scheme 1. Representative Molecular Motors and Their Rotation Rates Expressed in Terms of the Half-Life of the Thermal Step ($t_{1/2}$) at Room Temperature**

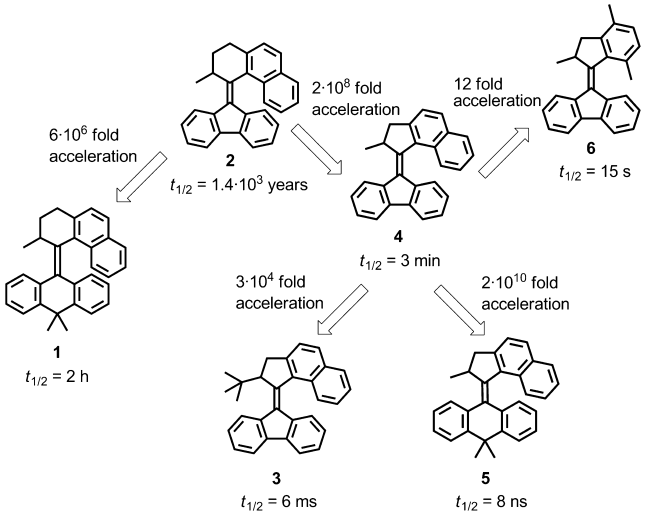


the second-generation motor instead of a six-membered ring increased the rotation rate dramatically.[20,21] The analogous change in ring size in the lower half, however, had an opposite effect.[26] Changing the naphthyl group in the upper half to a *p*-xylyl group[27] or a benzothiophene group[28] also caused faster rotation. Furthermore, increasing the steric bulk of the substituent at the stereogenic center was shown to accelerate the rotation.[20,21,29]

We have devoted continuing efforts toward designing faster molecular motors.[20,21,35] Scheme 1 shows a number of structural changes that have been used to achieve this by, for example, changing the ring sizes, the substituents at the stereogenic center, or the aromatic parts.

In our pursuit of faster motors, we are interested in learning how many of these structural effects may simultaneously be incorporated into the design and still give a faster motor. As part of the gradual incorporation of structural features that cause acceleration of the motor, we envisioned preparing and studying molecular motors **7** and **17** as our next design (Figure 1). Motor **4**, as shown in Scheme 1, may be accelerated either

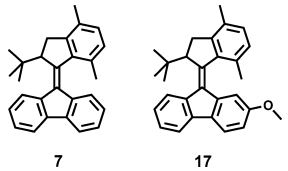


**Figure 1.** New design of the molecular motor.

by replacing its naphthyl moiety with a xylyl moiety (motor **6**) or by replacing the methyl substituent with a bulkier *tert*-butyl substituent (motor **3**). Motor **7** (our target molecule) and its desymmetrized analogue **17** may be viewed as having the best of both worlds: both the xylyl moiety and the *tert*-butyl substituent. As shown in Scheme 1, both structural variations seem to accelerate motor **4** individually. With our initial design of motor **7**, we aimed to examine how these two "accelerating structural variations" act together. Is the new motor **7** faster than motor **4**? Is it faster than motors **3** and **6**? Do the accelerating effects cumulate? Does this system retain its unidirectional nature? These are the key questions we set out to address.

## RESULTS AND DISCUSSION

**Synthesis and Characterization.** Overcrowded alkene **7** was synthesized according to Scheme 2. Ketone **9** was prepared by sequential Friedel−Crafts acylation and alkylation reactions on *p*-xylene (**8**) following a literature procedure.[30,31] Introducing the *tert*-butyl group at the $\alpha$-position of ketone **9** required two reaction steps following a procedure for the conversion of cyclopentanone to 2-*tert*-butylcyclopentanone:[32] the ketone was first converted to the TMS-protected enol **10**, which was then reacted with *t*-BuCl in the presence of $TiCl_4$ to give the upper-half ketone **11**. Thioketone **12** was prepared by reaction of the ketone with $P_4S_{10}$ and proved to be remarkably stable; thioketones prepared for the synthesis of motors are normally quite unstable and are therefore immediately used in the next step.[33] Thioketone **12** however, could be stored for weeks if free of residual $P_4S_{10}$. We reason that the *t*-Bu and Me groups "protect" the thioketo group, rendering it unreactive. Preparing the lower half of the motor was straightforward. Fluorenone (**13**) was converted into hydrazone **14**, which was oxidized with $MnO_2$ to give diazofluorenone (**15**). The crucial step of the synthesis was the diazo−thioketone coupling (Barton−Kellogg reaction),[29] which provided **16** in moderate yield. Episulfide **16** was desulfurized with $P(C_6H_5\text{-OMe-}p)_3$ to give the overcrowded alkene **7**.[29] This more polar phosphine was employed instead of the more commonly used $PPh_3$ because this allowed easier separation of the formed $S{=}PAr_3$ and the residual $PAr_3$ from the desired product.

All of the synthetic intermediates and the target overcrowded alkene **7** were fully characterized by $^1$H NMR and attached proton test (APT) $^{13}$C NMR spectroscopic techniques as well as by high-resolution mass spectrometry (HRMS). In HRMS, the final product **7** gave a peak corresponding to the protonated molecule **7**, $[M + H]^+$. A characteristic pattern of three signals from the aliphatic ring protons of the five-membered-ring upper half described earlier for similar overcrowded alkenes[29] was also found in the $^1$H NMR spectrum of the final product. In addition, the signals from the carbon atoms of the central C=C bond were present in the APT NMR spectrum in the region from 131 to 152 ppm.

Overcrowded alkene **17** was prepared through a synthetic pathway analogous to that for motor **7** (Scheme 3). Once more the crucial step in the synthesis was the diazo−thioketone coupling (Barton−Kellogg reaction), which was carried out in good yield. During purification of the resulting episulfides, it was possible to collect a batch that mostly contained the isomer *E*-**21** and another one that mainly contained the isomer *Z*-**21**. These isomers were separately reacted under the desulfurization conditions (in the absence of light) in order to establish whether the desulfurization step takes place in a stereoselective fashion. Both reactions, however, gave a mixture of *E*-**17** and *Z*-**17** in the ratio of 1:1 and are therefore not stereoselective. Molecular motors *E*-**17** and *Z*-**17** were not separable by column chromatography on silica or by crystallization. However, the isomers could be separated by preparative HPLC.

Product **17** and the synthetic intermediates were fully characterized by $^1$H NMR and APT NMR spectroscopic techniques as well as by HRMS. The configuration about the


dx.doi.org/10.1021/jo500411z | J. Org. Chem. 2014, 79, 4446−4455

**Scheme 2. Synthesis of Overcrowded Alkene 7**

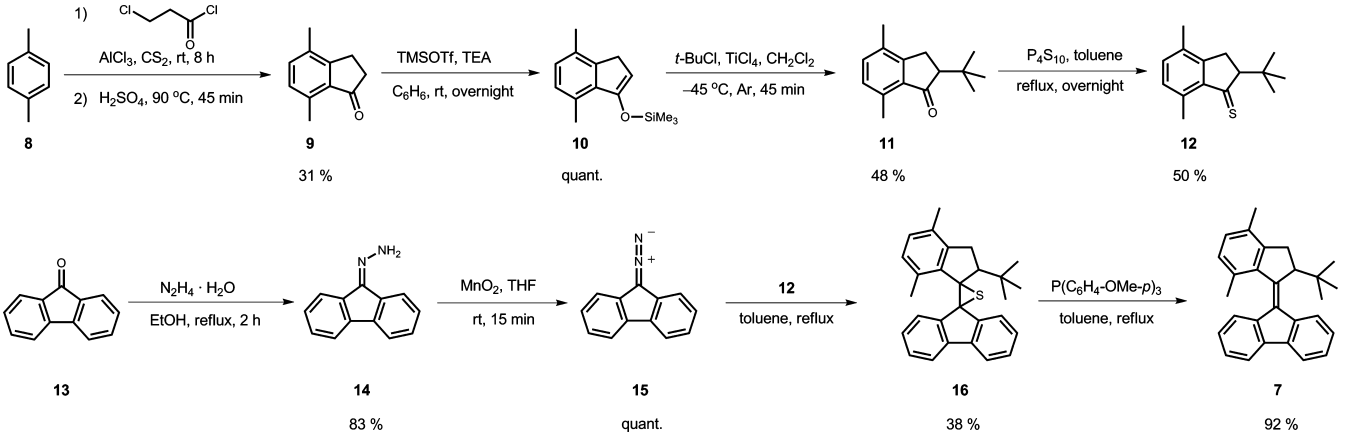


**Scheme 3. Synthesis of Overcrowded Alkene 17**

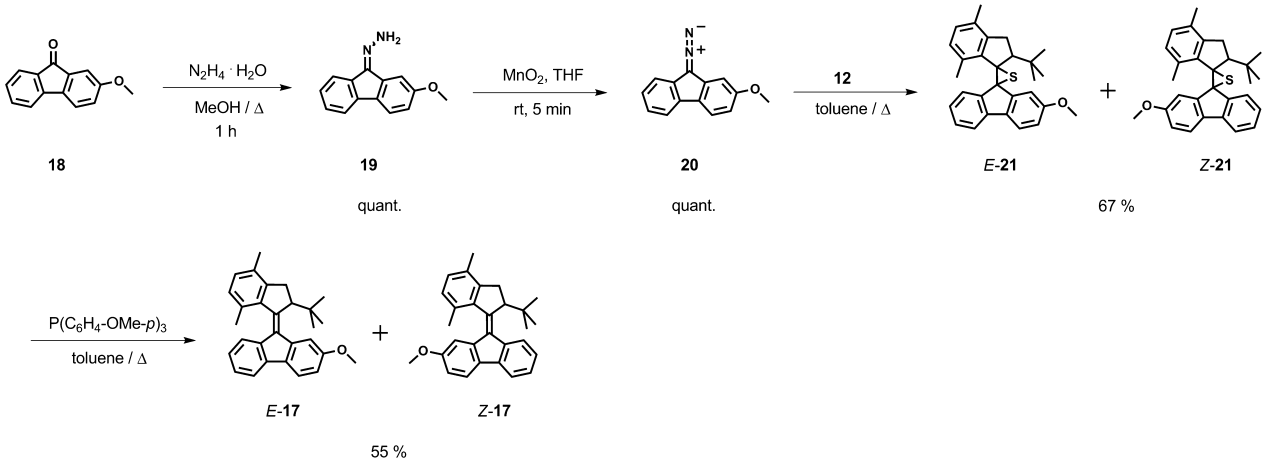


central double bond, however, could not be deduced from the $^1$H NMR and APT spectra of the two isomers of **17**. Both isomers were therefore analyzed by 2D NOESY NMR techniques. The structures of both isomers of **17** as well as the crucial NOE contacts are depicted in Figure 2. The *E* isomer shows an NOE contact of the only aromatic proton giving a singlet in the $^1$H NMR spectrum (proton o in Figure 2) with the proton at the stereogenic center (proton f in Figure 2) as well as a contact with the protons of the *tert*-butyl group (protons g in Figure 2). The upper-half protons f and g come into spatial proximity only with the lower-half proton o in isomer *E*-**17**. The other isomer shows an NOE contact of a lower-half aromatic proton that gives a doublet in the $^1$H NMR spectrum with proton f in the upper half as well as a contact with protons g in the upper half. These contacts are possible only for the aromatic proton h in the lower half of isomer *Z*-**17** (Figure 2).

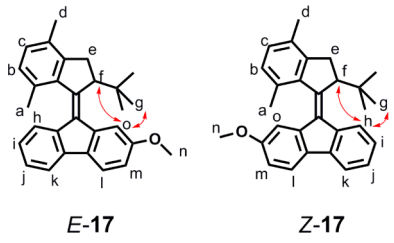


**Figure 2.** Structures of *E*-**17** and *Z*-**17** and the NOE contacts revealing their configurations about the central C=C bond.

**Photochemical Properties.** The UV–vis spectrum of overcrowded alkene **7** in isopentane at −85 °C is shown in Figure 3. Upon irradiation with 365 nm light, the band at $\lambda_{max}$ = 350 nm in the UV–vis spectrum disappears, and at the same time a new band appears at $\lambda_{max}$ = 430 nm. This also reveals an

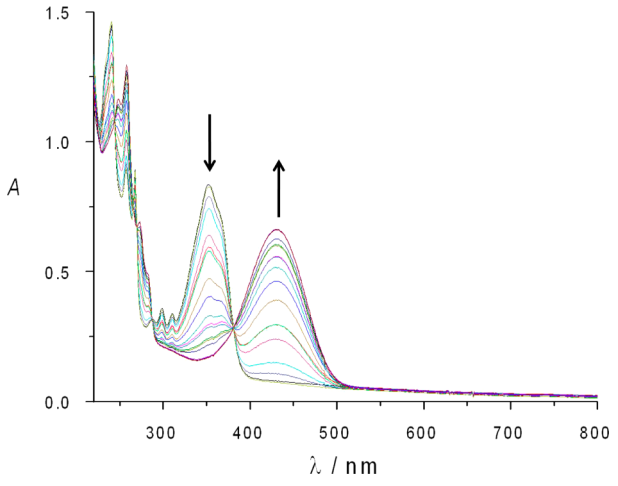


**Figure 3.** UV–vis spectra of motor **7** ($c$ = 2.1 × 10$^{-5}$ mol dm$^{-3}$ in isopentane) at −85 °C upon irradiation at $\lambda$ = 365 ± 30 nm.


dx.doi.org/10.1021/jo500411z | J. Org. Chem. 2014, 79, 4446–4455

isosbestic point at 380 nm. These changes were not observed at room temperature. The described process is completely reversible upon irradiation with visible light ($\lambda$ > 420 nm) at −85 °C or when the temperature is raised to room temperature to allow the thermal process to take place. These processes correspond to the stable form of motor **7** undergoing photochemical isomerization to give a mixture of the stable and unstable forms at the photostationary state (PSS) and the photochemical or thermal conversion of the unstable form back to the stable form of motor **7**, as shown in Scheme 4.

**Scheme 4. Rotation Cycle of Motor (*R*)-7**

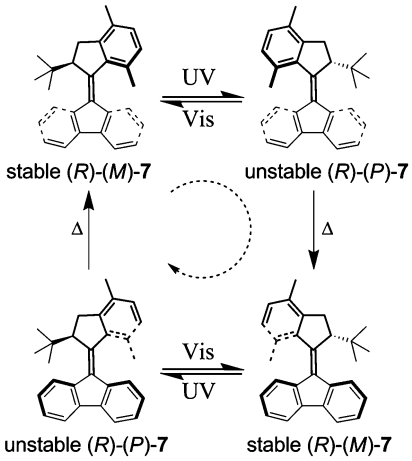


The same processes could also be followed by CD spectroscopy, for which the two enantiomers of motor **7** were resolved. This was achieved by chiral preparative HPLC. As expected, the two enantiomers gave CD spectra of opposite sign. Only one enantiomer was chosen for further experiments. In Figure 4, the CD spectrum of the chosen enantiomer of

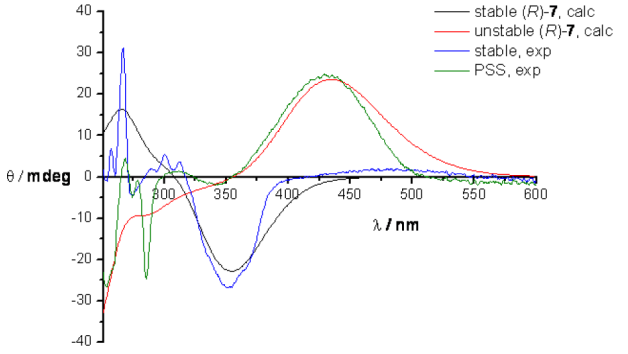


**Figure 4.** Experimental CD spectra of the chosen enantiomer of motor **7** and the PSS reached with 365 nm light, taken in isopentane ($c$ = 2.7 × $10^{-5}$ mol $dm^{-3}$), and calculated CD spectra for (*R*)-**7** obtained using TD-DFT at the B3LYP/6-31G(d,p) level.

motor **7** is compared to the calculated CD spectrum of (*R*)-(*M*)-**7**, which is the stable form of (*R*)-**7** (*R* defines the absolute configuration at the stereogenic center in **7**). The spectra agree well, confirming the absolute configuration of the stereogenic center of the chosen enantiomer of motor **7** as (*R*). Furthermore, the CD spectrum of **7** at the PSS reached by irradiation of the chosen enantiomer of motor **7** with 365 nm light at −150 °C compares well to the calculated CD spectrum of (*R*)-(*P*)-**7**, which is the unstable form of the (*R*)-**7**. The CD spectra were calculated in the gas phase by time-dependent density functional theory (TD-DFT) using a hybrid functional (B3LYP) with the 6-31G(d,p) basis set.

The switching process of (*R*)-**7** was investigated by CD spectroscopy, as depicted in Figure 5. The measurements were

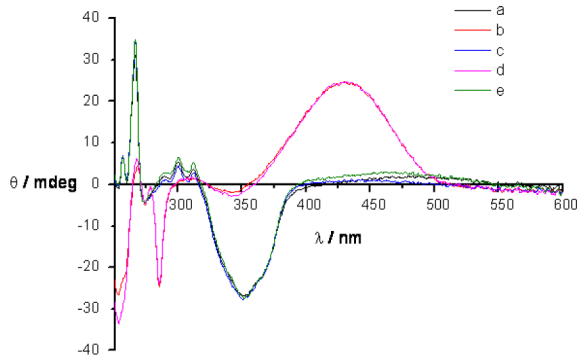


**Figure 5.** CD spectra of (*R*)-**7** in isopentane ($c$ = 2.7 × $10^{-5}$ mol $dm^{-3}$) to follow the photochemical and thermal steps: (a) sample at 123 K in the absence of light; (b) sample at 123 K at the PSS (after irradiation with UV light at 365 nm for 45 min); (c) sample in (b) after irradiation with visible light at $\lambda$ > 420 nm for 1.25 h at 123 K; (d) sample in (c) after irradiation to the PSS (irradiation with UV light at 365 nm for 35 min) at 123 K; (e) sample in state (d) after warming to 243 K and then cooling to 123 K again.

performed at −150 °C to prevent any thermal processes on the time scale of the experiments. Irradiation at 365 nm caused the disappearance of the CD signal at $\lambda_{max}$ = 350 nm and the appearance of a new CD signal at $\lambda_{max}$ = 430 nm. The positions of the two interconverting CD bands correspond to the positions of the two interconverting UV−vis bands in terms of wavelength, $\lambda_{max}$ (Figure 3). The two CD bands are of the opposite sign, however, indicating a change in the helicity of the motor. This corresponds to reaching the PSS upon irradiation at 365 nm. This process can be reversed either photochemically or thermally, as irradiation with visible light at $\lambda$ > 420 nm or warming to −30 °C restored the original CD spectrum (Figure 5).

The CD experiments show that the overcrowded alkene **7** changes its helicity in the photochemical step as well as in the thermal step (Figure 5), in accordance with the isomerization processes depicted in Scheme 4.

The rotation cycle of a motor comprises two photochemical and two thermal steps. For a motor with a symmetrical lower half, the rotation cycle has two identical photochemical steps and two identical thermal steps (Scheme 4). The photochemical steps of rotary motors are fast,[34] and the thermal steps are slow and therefore rate-determining. The rotation rate of motors is thus expressed by the half-life of the thermal step at room temperature. Determining the half-life of the thermal step at room temperature requires either that the reaction kinetics be followed at room temperature or that the kinetic data be extrapolated from the temperatures used. For a fast motor like **7**, following the reaction kinetics at room temperature can prove impossible using a standard spectroscopic technique such as UV−vis, CD, or NMR spectroscopy because at room temperature the thermal step is much too fast to be measured by those techniques. A way to come around this, as mentioned above, is to perform the measurements at low temperatures where the reaction is slow enough to be followed by these spectroscopic techniques. The data collected at different (low)


dx.doi.org/10.1021/jo500411z | J. Org. Chem. 2014, 79, 4446−4455

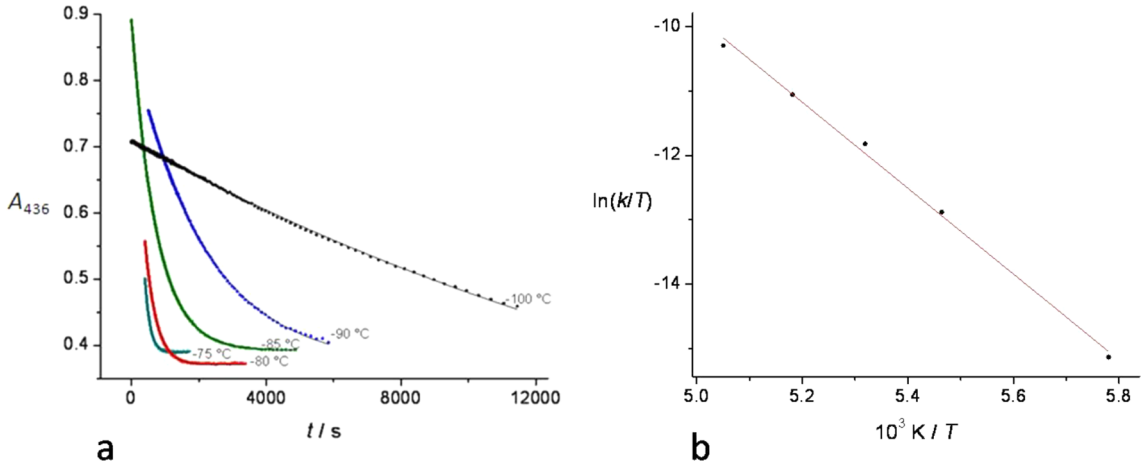


**Figure 6.** (a) Thermal relaxation of motor **7** in the dark after it reached the PSS upon irradiation at $\lambda$ = 365 ± 30 nm ($c = 2.1 \times 10^{-5}$ mol dm$^{-3}$ in isopentane) at various temperatures: (●) experimental data; (—) data calculated by means of regression analysis. (b) Analysis of the data from Table 1 by means of the Eyring equation: (●) experimental data; (—) data calculated by means of regression analysis.

temperatures can then be extrapolated to give the half-life at room temperature.[35]

We followed the reaction by low-temperature UV−vis spectroscopy. A solution of motor **7** in isopentane was irradiated with UV light ($\lambda$ = 365 nm) at −150 °C until the PSS was reached. The rate of thermal isomerization was then followed by UV−vis spectroscopy at five different temperatures in the range between −75 and −100 °C. The data are shown in Figure 6a. The data were fitted to a first-order rate law exponential function by nonlinear regression analysis. The resulting half-lives at the measured temperatures are given in Table 1. The values were determined to be between 2 and 250 min over the temperature range between −75 and −100 °C.

**Table 1. Half-Lives ($t_{1/2}$) for Motor 7 at Different Temperatures Obtained from Regression Analysis of the Data in Figure 6a**

| $T$/°C | $t_{1/2}$/min | $R^2$ |
|---|---|---|
| −75 | 1.7 | 0.99955 |
| −80 | 3.8 | 0.99977 |
| −85 | 8.4 | 0.99992 |
| −90 | 25 | 0.99382 |
| −100 | 250 | 0.99898 |

The data in Table 1 were fitted to the Eyring equation, from which the activation enthalpy ($\Delta^{\ddagger}H^{\circ}$ = 55 ± 1.7 kJ mol$^{-1}$) and activation entropy ($\Delta^{\ddagger}S^{\circ}$ = −1.3 ± 9.4 J K$^{-1}$ mol$^{-1}$) were calculated (Figure 6b). These parameters allow for the extrapolation of the data to room temperature. The half-life of the thermal step was in this way determined to be 1 ms at room temperature. These values were derived from the measurements carried out in isopentane.

This value was obtained by extrapolation over a large temperature range (around 100 K) and the extrapolation was carried out over a logarithmic scale, which may introduce a significant error. Furthermore, one cannot exclude the possibility that the motor exhibits different behavior at low temperatures than at room temperature. For these reasons it was necessary to check the value obtained from the low-temperature kinetic study. The use of a technique that could be used at room temperature would be beneficial, as it would allow us to measure the kinetics directly at and around room temperature and would speed up the experiments because the reaction proceeds much faster at room temperature. We then turned to the use of transient absorption to follow the thermal step around room temperature. This technique is able to record light intensity with high time resolution to allow very fast processes to be followed.[35]

Transient absorption was used to follow the thermal step in *n*-heptane over the temperature range from 15 to 45 °C. A representative transient absorption trace is shown in Figure 7a (other traces can be found in the Supporting Information). The data were fitted to a first-order rate law exponential function to obtain the half-lives at the measured temperatures (Table 2). The data obtained were analyzed using the Eyring equation (Figure 7b), from which the parameters $\Delta^{\ddagger}H^{\circ}$ = 55 ± 1.1 kJ mol$^{-1}$ and $\Delta^{\ddagger}S^{\circ}$ = −12 ± 4 J K$^{-1}$ mol$^{-1}$ were calculated. These were used to calculate the half-life at room temperature, and the value $t_{1/2}$ = 3 ms was obtained. These values agree well with those obtained by the UV−vis spectroscopic study at low temperatures.

The values of the half-life at room temperature obtained by low-temperature UV−vis spectroscopy ($t_{1/2}$ = 1 ms, measured in isopentane) and transient absorption ($t_{1/2}$ = 3 ms, measured in *n*-heptane) compare very well. This shows that the kinetics of the thermal step may reliably be followed by either of the two techniques. For fast molecular motors such as **7**, it is more practical and less time-consuming to follow the process at room temperature by transient absorption spectroscopy.

Furthermore, our results show that motor **7** exhibits the same behavior in the thermal step at low temperature as it does at room temperature, justifying the process of extrapolation used to obtain the half-life at room temperature from the low-temperature UV−vis study.

Motor **7** may now be compared with other motors from Scheme 1 on the basis of the half-lives at room temperature (the average of the two experimentally determined values for motor **7** is taken for the comparison). Motor **7** is faster than motor **4** by a factor of $10^5$ and is also $10^4$ times faster than motor **6** and 4 times faster than motor **3**. From this we conclude that the introduction of two "accelerating structural features" to motor **4** makes it indeed faster than adding either one of them alone. By simply multiplying the accelerating effects from Scheme 1 (for going from motor **4** to motor **3** and from **4** to **6**), one could roughly predict 4 × $10^5$-fold


dx.doi.org/10.1021/jo500411z | J. Org. Chem. 2014, 79, 4446−4455

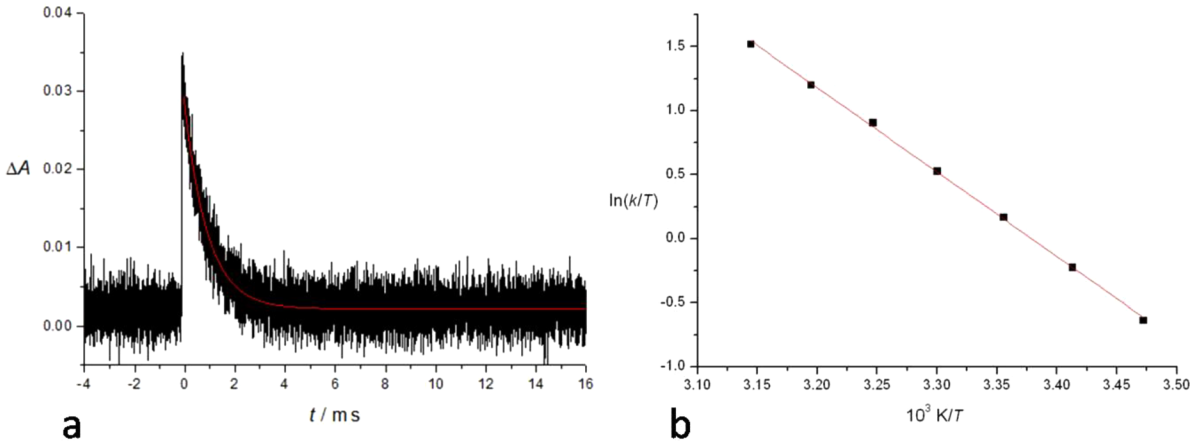


**Figure 7.** (a) Transient absorption measurements performed on motor **7** in *n*-heptane at 35 °C. The PSS was reached with a 355 nm laser (3 mJ per pulse), and the absorbance at 430 nm was followed. Experimental data are given in black, and the red line shows data calculated by means of regression analysis. (b) Analysis of the data from the transient absorption measurements by means of the Eyring equation: (■) experimental data; (—) data calculated by means of regression analysis.

**Table 2. Half-Lives ($t_{1/2}$) for Motor 7 at Different Temperatures Obtained from Regression Analysis of the Data Obtained by Transient Absorption**

| $T$/°C | $t_{1/2}$/ms |
|---|---|
| 15 | 4.6 |
| 20 | 2.9 |
| 25 | 2.0 |
| 30 | 1.4 |
| 35 | 0.9 |
| 40 | 0.7 |
| 45 | 0.5 |

acceleration for going from motor **4** to motor **7**. Such a rough "prediction" actually turns out to be quite close to the acceleration of $10^5$ that we observed experimentally.

Gas-phase theoretical investigations [DFT B3LYP/6-31G-(d,p)] of the unstable and stable forms of motor **7** as well as of the transition state for the thermal process between the two forms were also conducted. The calculated value of the activation free energy for the thermal process determined from the vibrational analysis, $\Delta^{\ddagger}G^{\circ}$ = 58 kJ mol$^{-1}$, is in good agreement with the experimentally determined ones (55 ± 4 and 58 ± 3 kJ mol$^{-1}$ at room temperature, as determined by UV−vis spectroscopy in isopentane and transient absorption spectroscopy in *n*-heptane, respectively). The half-life at room temperature was calculated to be $t_{1/2}$ = 2.2 ms, also in good agreement with the experimentally determined values.

In order to perform continuous work, a rotary molecular motor should exhibit unidirectional rotation. The rotary motion of a new motor should therefore be tested for unidirectionality. Motor **7**, however, is not suitable for this because it has only one stable and one unstable form as a result of its symmetrical lower half, so there is no way of telling which direction the rotation adopts in going from the unstable to the stable form. For that reason, we designed molecular motor **17** bearing a nonsymmetrical lower half; this molecule has two distinct stable forms and two distinct unstable forms, as shown in Scheme 5. It should now be possible to observe which unstable form thermally relaxes into which stable form and whether the overall rotary process is indeed unidirectional.

As mentioned above, in order to confirm unidirectionality of the rotation process, one needs to study the directionality of

**Scheme 5. Rotation Cycle of Motor (*R*)-17**

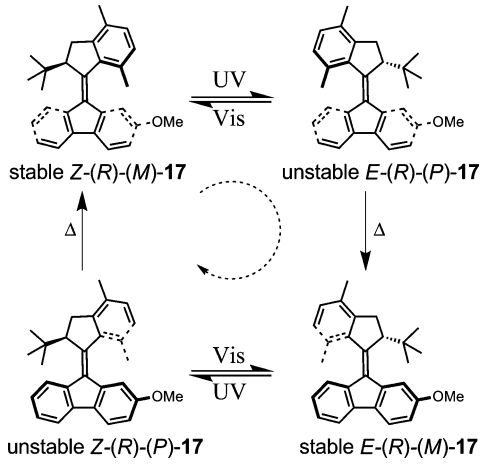


the two thermal steps (Scheme 5). This means one needs to compare the composition of the mixture after each thermal step to the composition of the mixture prior to the thermal step (i.e., after the photochemical step, at the PSS). The composition of the mixture after the thermal process (i.e., the ratio of the stable *E* and *Z* forms of **17**) can easily be determined by HPLC analysis. The composition of the mixture at the PSS (i.e., the ratio of the unstable and stable forms of **17**), however, is more difficult to determine because the PSS is reached at −150 °C to prevent the unstable form from undergoing the thermal process. These thermal processes were determined computationally to have barriers of $\Delta^{\ddagger}G^{\circ}$ = 58.2 and 56.0 kJ mol$^{-1}$ for *Z*-(*R*)-**17** and *E*-(*R*)-**17**, respectively, which are similar to the experimentally and computationally obtained values for compound **7**. Analysis of the PSS mixture at that temperature would be extremely difficult to carry out. However, a method developed by Fischer allows for the estimation of the composition at the PSS from UV−vis spectra by irradiation of the sample at two different wavelengths (in two separate experiments).[36] The method is based on the assumption that the ratio of the quantum yields of the starting and newly formed species is independent of the wavelength used to reach the PSS, therefore allowing the composition at the PSS to be


dx.doi.org/10.1021/jo500411z | J. Org. Chem. 2014, 79, 4446−4455

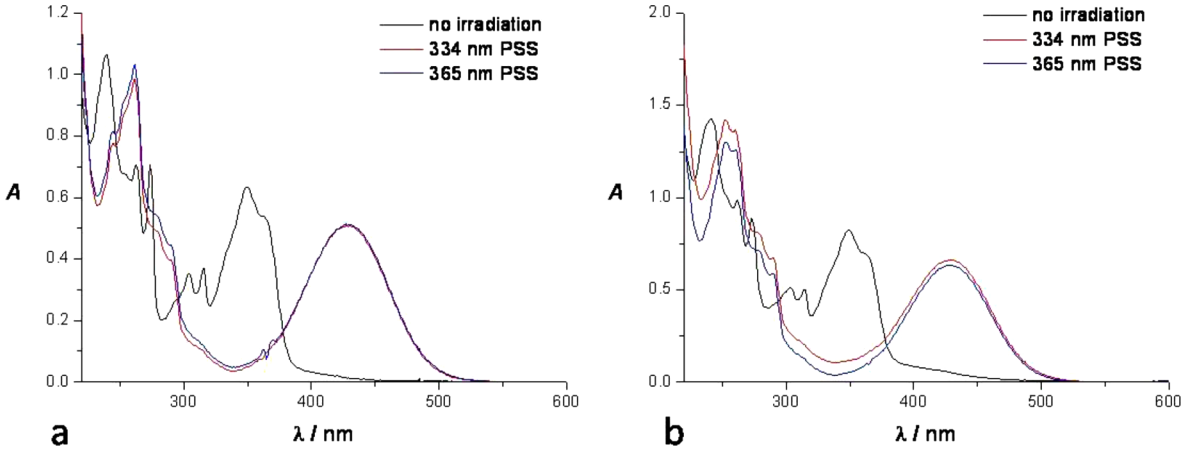


**Figure 8.** UV−vis spectra of (a) *Z*-**17** and (b) *E*-**17** taken in isopentane ($c = 2.0 \times 10^{-5}$ mol dm$^{-3}$) at −150 °C. Irradiation was performed at −150 °C.

calculated from the difference in the UV−vis spectra taken at the two PSSs.

Figure 8 shows the UV−vis spectra of the stable forms of **17** as well as of the PSS mixtures reached by irradiation at two different wavelengths, namely, 334 and 365 nm. Using the data from Figure 8, one can apply Fischer's method[36] to estimate the compositions of the mixtures at the PSSs. Irradiating *E*-**17** at 334 nm gives the unstable form of *Z*-**17** and the stable form of *E*-**17** in a 96:4 ratio, and irradiating at 365 nm gives a ratio of 97:3. Irradiating *Z*-**17** at 334 and 365 nm gave more than 98% of the unstable form at both wavelengths. Motor **17** appears to have a remarkably high content of the unstable form at the PSS, which is a prerequisite for good working efficiency. This finding is also supported by the UV−vis and CD studies of **7**, which showed almost complete conversion of the stable form to the unstable form (Figures 4−6).

The samples irradiated to the PSS were then warmed to room temperature and subsequently analyzed by HPLC to determine the contents of the mixture, namely, the ratio of the stable *E* and *Z* forms of **17**. The sample of *Z*-**17** that had been irradiated to the PSS with 334 nm light (more than 98% of the unstable form) and was then allowed to warm up contained the stable forms of *E*-**17** and *Z*-**17** in a 96:4 ratio. The same result was obtained with 365 nm light. The sample of *E*-**17** that had been irradiated to the PSS with 334 nm light (containing the unstable form of *Z*-**17** and the stable form of *E*-**17** in a 96:4 ratio) and was then allowed to warm up contained the stable forms of *Z*-**17** and *E*-**17** in a ratio of 96:4. The sample of *E*-**17** that had been irradiated to the PSS with 365 nm light (containing the unstable form of *Z*-**17** and the stable form of *E*-**17** in a 97:3 ratio) and was then allowed to warm up contained the stable forms of *Z*-**17** and *E*-**17** in a ratio of 93:7. The ratios of the stable *E* and *Z* forms of **17** correspond well with the estimated ratios of the stable and unstable forms of **17** at the PSSs. These results show that practically all of the unstable form of *Z*-**17** is thermally converted to the stable form of *Z*-**17**and that the unstable form of the *E* isomer is thermally converted to the stable *E* form (Scheme 5). This proves the unidirectionality of the thermal steps and therefore also confirms the unidirectionality of the entire rotatory cycle.

We have shown that the thermal steps are highly efficient (all of the unstable forms convert to a single stable form), as are the photochemical steps (very high content of the unstable form). These findings reflect the high efficiency of motor **17** in performing unidirectional rotation.

## ■ CONCLUSION

The elucidation of the key structural parameters that govern the rotary speed of light-driven molecular motors is paramount for the design of future systems based on these molecules. To this end, we have successfully synthesized a new molecular motor comprising a fluorene lower half and a five-membered-ring upper half; the upper-half ring is fused to a *p*-xylyl moiety and bears a *tert*-butyl group at the stereogenic center. The photochemical and thermal behavior of the motor was studied by low-temperature UV−vis and CD spectroscopic techniques. The kinetics of the thermal isomerization were studied by low-temperature UV−vis spectroscopy as well as by transient absorption spectroscopy at room temperature, and the half-life of the process at room temperature was determined to be 1 and 3 ms, respectively. The values are in very good agreement. In accordance with our predictions, the molecular motor shows $10^4$ times faster rotation than its analogue bearing a methyl group at the stereogenic center instead of a *tert*-butyl group. It is also 4 times faster than the analogue with a naphthyl group fused to the upper-half five-membered ring instead of a *p*-xylyl group. This shows that the *tert*-butyl and *p*-xylyl groups on the upper-half five-membered ring may be used simultaneously in the same molecular design to achieve an acceleration of the rotation rate of the molecular motor that is larger than the acceleration obtained by using either one of the two groups individually.

A 2-methoxyfluorene derivative of the new molecular motor was also synthesized with the purpose of studying the directionality of the motor's rotation. The new molecular motor shows remarkably high PSSs (above 96% of the unstable form upon irradiation) as well as unidirectional rotation. These properties make this molecular design highly promising for use in future applications where molecular motors will be utilized to deliver work.

## ■ EXPERIMENTAL SECTION

**General Remarks.** Solvents were reagent-grade and were distilled and dried before use according to standard procedures. For physicochemical measurements, Uvasol-grade solvents from Merck were used. Reactions were performed under a nitrogen atmosphere unless specified otherwise. Analytical TLC was performed with Merck


dx.doi.org/10.1021/jo500411z | J. Org. Chem. 2014, 79, 4446−4455

silica gel 60 F254 plates, and visualization was accomplished by UV light. Column chromatography was performed on silica gel (Aldrich 60, 230−400 mesh). $^1$H NMR spectra were recorded on 400 or 500 MHz NMR spectrometers. $^{13}$C NMR spectra were recorded on 100 or 125 MHz NMR spectrometers. Chemical shifts ($\delta$) are denoted in parts per million relative to $CDCl_3$ (for $^1$H detection, $\delta$ = 7.26 ppm; for $^{13}$C detection, $\delta$ = 77.16 ppm) or $CD_2Cl_2$ (for $^1$H detection, $\delta$ = 5.32 ppm; for $^{13}$C detection, $\delta$ = 53.50 ppm). For $^1$H NMR spectroscopy, the splitting pattern of peaks is designated as follows: s (singlet), d (doublet), t (triplet), q (quartet), m (multiplet), br (broad), or dd (doublet of doublets). HRMS spectra were obtained on an LTQ Orbitrap XL mass spectrometer with ESI, APCI, or APPI ionization. Cryo-UV−vis and CD measurements were performed using a variable-temperature liquid nitrogen cryostat inserted into an FT spectrophotometer or a spectropolarimeter. Transient absorption experiments were performed using a Nd:YAG laser (FWHM, 8 ns; 355/532/1064 nm; up to 600 mW), a xenon lamp (250−800 nm, using a 200−2500 nm monochromator with an accuracy of 0.2 nm), and a 185−900 nm PMT detector. Irradiation experiments with UV light were performed using an ENB-280C/FE lamp with $\lambda$ = 312 ± 30 or 365 ± 30 nm or a 200 W Hg lamp fitted with suitable bandpass filters (typical bandwidth of 10 nm). Irradiation experiments with visible light were performed using suitable cutoff filters.

**Syntheses.** *(4,7-Dimethyl-1H-inden-3-yloxy)trimethylsilane (**10**).* To a stirred solution of ketone **9**[30,31] (3.0 g, 19 mmol) and $Et_3N$ (8.0 mL, 57 mmol) in benzene (60 mL) under a nitrogen atmosphere was added TMSOTf (8.0 mL, 46 mmol), and the resulting mixture was stirred overnight at room temperature. The progress of the reaction was followed by TLC (*n*-pentane/AcOEt 30:1), but care had to be taken as the product decomposed on silica. The reaction was quenched by the addition of a saturated aqueous $NaHCO_3$ solution (50 mL). The organic layer was separated, and the aqueous layer was washed with *n*-pentane (3 × 20 mL). The combined organic layers were dried on anhydrous $Na_2SO_4$. After filtration, the solvent was evaporated to afford a brown liquid that solidified upon standing. A $^1$H NMR spectrum of the crude intermediate showed the complete conversion of ketone **9** into intermediate **10**, which was used in the next step without further purification. $^1$H NMR (400 MHz, $CDCl_3$): $\delta$ 7.04 (d, *J* = 7.6 Hz, 1H), 7.00 (d, *J* = 7.6 Hz, 1H), 5.47 (t, *J* = 1.8 Hz, 1H), 3.19 (d, *J* = 1.8 Hz, 2H), 2.65 (s, 3H), 2.38 (s, 3H), 0.40 (s, 9H). $^{13}$C NMR (100 MHz, $CDCl_3$): $\delta$ 155.7, 142.0, 138.4, 130.4, 129.1, 128.7, 126.5, 105.3, 32.7, 18.0, 17.7, 0.2.

*2-tert-Butyl-4,7-dimethyl-2,3-dihydro-1H-inden-1-one (**11**).* Crude compound **10** (obtained from 19 mmol of ketone **9**) was dissolved in dry dichloromethane (24 mL), which was degassed with argon, and 2.4 mL (21 mmol) of *t*-BuCl was added under an argon atmosphere. The solution was cooled to −50 °C, and $TiCl_4$ (2.4 mL, 21 mmol) was added in one portion. The reaction mixture was stirred at that temperature, and the progress of the reaction was monitored by TLC (*n*-pentane/AcOEt 30:1). After approximately 1 h, the reaction was quenched by the addition of water (50 mL) and dichloromethane (25 mL). The layers were separated, and the organic layer was washed once more with water and once with diluted aqueous $NaHCO_3$ solution. The organic solution was dried on anhydrous $Na_2SO_4$. After filtration, the solvent was evaporated to afford a brown liquid that was purified by column chromatography on silica using *n*-pentane/AcOEt 30:1 as the eluent. This afforded ketone **11** as a waxy off-white solid (2.0 g) in 48% yield. $^1$H NMR (400 MHz, $CDCl_3$): $\delta$ 7.22 (d, *J* = 7.4 Hz, 1H), 6.99 (d, *J* = 7.4 Hz, 1H), 3.02 (dd, *J* = 17.4, 8.1 Hz, 1H), 2.78 (dd, *J* = 17.4, 3.7 Hz, 1H), 2.58 (s, 3H), 2.44 (dd, *J* = 7.7, 4.4 Hz, 1H), 2.31 (s, 3H), 1.06 (s, 9H). $^{13}$C NMR (100 MHz, $CDCl_3$): $\delta$ 209.5, 152.9, 135.9, 135.1, 134.3, 132.5, 129.4, 56.9, 33.9, 28.6, 27.8, 18.3, 17.6. HRMS (ESI) *m*/*z*: calcd for $C_{15}H_{21}O^+$ 217.15924 $[M + H]^+$, found 217.15877 $[M + H]^+$.

*2-tert-Butyl-4,7-dimethyl-2,3-dihydro-1H-inden-1-thione (**12**).* Ketone **11** (614 mg, 2.84 mmol) was dissolved in dry toluene (60 mL), and $P_4S_{10}$ (14.0 g, 31.5 mmol) was added to the solution. The reaction mixture was heated at reflux with stirring under a nitrogen atmosphere. After 18 h the mixture was cooled to room temperature and filtered over a plug of silica (the silica was flushed with more toluene until all of the green component was collected). After removal of the solvent, the crude thioketone was purified by column chromatography on silica using *n*-pentane/toluene 7:1 as the eluent. Product **12** was collected as a dark-blue liquid (327 mg) in 50% yield and stored at −24 °C under an argon atmosphere. $^1$H NMR (400 MHz, $CDCl_3$): $\delta$ 7.21 (d, *J* = 7.5 Hz, 1H), 7.01 (d, *J* = 7.5 Hz, 1H), 3.04 (s, 3H), 2.68 (s, 3H), 2.35 (s, 3H), 0.97 (s, 9H). $^{13}$C NMR (100 MHz, $CDCl_3$): $\delta$ 250.1, 152.9, 145.0, 136.6, 133.5, 132.0, 130.7, 71.2, 35.3, 33.1, 28.0, 21.7, 18.2. HRMS (ESI) *m*/*z*: calcd for $C_{15}H_{21}S^+$ 233.13640 $[M + H]^+$, found 233.13602 $[M + H]^+$.

*Dispiro[9H-fluorene-9,2′-thiirane-3′,1″-(2″-tert-butyl-4″,7″-dimethyl-2″,3″-dihydro-1H-indene)] (**16**).* Thioketone **12** (50 mg, 0.22 mmol) and diazofluorenone (**15**) (83 mg, 0.44 mmol) were dissolved in dry toluene (20 mL) under a nitrogen atmosphere, and the mixture was stirred at 70 °C for 1 h. The temperature of the solution was slowly increased until reflux. The reaction ran overnight at reflux and was followed by TLC (*n*-pentane/AcOEt 300:1). Upon depletion of the starting compounds **12** and **15**, the solvent was evaporated. The crude product was first purified by column chromatography on silica with *n*-pentane/toluene 11:1 as the eluent and then by crystallization from *n*-heptane. Episulfide **16** was obtained as a white solid (32 mg) in 38% yield. $^1$H NMR (500 MHz, $CDCl_3$): $\delta$ 7.71 (d, *J* = 7.3 Hz, 1H), 7.62 (d, *J* = 7.5 Hz, 1H), 7.52 (d, *J* = 7.6 Hz, 1H), 7.39 (t, *J* = 7.0 Hz, 1H), 7.32 (t, *J* = 7.5 Hz, 1H), 7.18 (t, *J* = 7.2 Hz, 1H), 7.09 (d, *J* = 7.8 Hz, 1H), 6.95 (t, *J* = 7.6 Hz, 1H), 6.81 (d, *J* = 7.7 Hz, 1H), 6.77 (d, *J* = 7.7 Hz, 1H), 2.83 (s, 3H), 2.71 (d, *J* = 6.2 Hz, 1H), 2.42 (d, *J* = 15.7 Hz, 1H), 2.03 (dd, *J* = 15.7, 6.2 Hz, 1H), 1.97 (s, 3H), 0.87 (s, 9H). $^{13}$C NMR (125 MHz, $CDCl_3$): $\delta$ 145.7, 144.3, 142.4, 141.2, 141.2, 139.1, 132.8, 130.4, 129.6, 128.9, 127.9, 127.6, 126.6, 126.2, 126.0, 124.4, 120.0, 119.6, 61.0, 56.3, 51.6, 34.6, 31.6, 29.2, 20.9, 18.2. HRMS (ESI) *m*/*z*: calcd for $C_{28}H_{29}S^+$ 397.19900 $[M + H]^+$, found 397.19827 $[M + H]^+$.

*9-(2-tert-Butyl-4,7-dimethyl-2,3-dihydro-1H-inden-1-ylidene)-9H-fluorene (**7**).* Episulfide **16** (32 mg, 0.08 mmol) was dissolved along with $P(C_6H_5\text{-}OMe\text{-}p)_3$ (35 mg, 0.10 mmol) in dry toluene (10 mL), and the stirred mixture was heated at reflux overnight under a nitrogen atmosphere. The solvent was evaporated, and the crude product was purified by column chromatography on silica with *n*-pentane/AcOEt 300:1 as the eluent. Pure **7** was obtained as a white solid (27 mg) in 92% yield. The enantiomers of **7** were separated by preparative chiral HPLC on an OD-H column with *n*-heptane/propane-2-ol 97:3 as the eluent at a flux of 0.5 mL min$^{-1}$. $^1$H NMR (500 MHz, $CD_2Cl_2$): $\delta$ 8.26 (dd, *J* = 5.5, 3.2 Hz, 1H), 7.83 (dd, *J* = 5.5, 3.2 Hz, 1H), 7.76 (d, *J* = 7.5 Hz, 1H), 7.47 (d, *J* = 7.9 Hz, 1H), 7.38 (dd, *J* = 5.7, 3.1 Hz, 2H), 7.30 (t, *J* = 7.4 Hz, 1H), 7.11 (m, 2H), 7.05 (d, *J* = 7.7 Hz, 1H), 4.22 (d, *J* = 5.6 Hz, 1H), 3.03 (dd, *J* = 15.0, 5.5 Hz, 1H), 2.86 (d, *J* = 15.0 Hz, 1H), 2.32 (s, 3H), 2.28 (s, 3H), 0.88 (s, 9H). $^{13}$C NMR (125 MHz, $CD_2Cl_2$): $\delta$ 152.2, 146.3, 142.6, 140.7, 139.8, 139.6, 138.5, 133.3, 130.9, 130.9, 130.4, 128.5, 127.5, 127.2, 126.9, 126.7, 125.4, 124.1, 119.8, 119.2, 58.6, 35.8, 35.5, 29.0, 20.7, 18.3. HRMS (ESI) *m*/*z*: calcd for $C_{28}H_{29}^+$ 365.22693 $[M + H]^+$, found 365.22620 $[M + H]^+$.

*(E,Z)-Dispiro[2-methoxy-9H-fluorene-9,2′-thiirane-3′,1″-(2″-tert-butyl-4″,7″-dimethyl-2″,3″-dihydro-1H-indene)] (E,Z-**21**).* Thioketone **12** (135 mg, 0.582 mmol) and diazofluorenone **20** (260 mg, 1.17 mmol) were dissolved in dry toluene (55 mL), and the mixture was heated at reflux under a nitrogen atmosphere overnight. The solvent was evaporated, and the crude product was purified by column chromatography on silica with *n*-pentane/toluene 3:1 as the eluent. Two fractions were collected, one containing predominantly one diastereoisomer of **21** (57 mg) and the other one containing predominantly the other diastereoisomer of **21** (110 mg). The crude products were immediately used in the next step without further purification. The overall crude yield of the reaction was 67%. HRMS (ESI) *m*/*z*: calcd for $C_{29}H_{31}OS^+$ 427.20956 $[M + H]^+$, found 427.20904 $[M + H]^+$.

*(E,Z)-9-(2-tert-Butyl-4,7-dimethyl-2,3-dihydro-1H-inden-1-ylidene)-2-methoxy-9H-fluorene (E,Z-**17**).* Episulfide **21** (first fraction; 57 mg, 0.13 mmol) and $P(C_6H_5\text{-}OMe\text{-}p)_3$ (60 mg, 0.17 mmol) were dissolved in dry toluene (20 mL), and the stirred mixture was heated at reflux overnight under a nitrogen atmosphere in the absence of light.


dx.doi.org/10.1021/jo500411z | J. Org. Chem. 2014, 79, 4446−4455

The solvent was evaporated, and the crude product was purified by column chromatography on silica using *n*-pentane/toluene 3:1 as the eluent, yielding a 1:1 mixture of *E*-**17** and *Z*-**17** (60 mg) as evident from $^1$H NMR analysis. The second fraction of episulfide **21** (110 mg, 0.26 mmol) underwent the same reaction and yielded a 1:1 mixture of *E*-**17** and *Z*-**17** (95 mg). The two batches of compound **17** were combined (quantitative crude yield). As no separation of the two isomers could be found by TLC, *E*-**17** and *Z*-**17** (14.5 mg total) were separated by preparative HPLC on an AD column with *n*-heptane/propane-2-ol 99:1 as the eluent at a flux of 1.0 mL min$^{-1}$. Because of the time-consuming process of separation of isomers by HPLC, only small amounts of the products *E*-**17** (4 mg) and *Z*-**17** (4 mg) were isolated in 55% yield. HRMS (ESI) *m*/*z*: calcd for $C_{29}H_{31}O^+$ 395.23749 $[M + H]^+$, found 395.23667 $[M + H]^+$. Data for *Z*-**17**: $^1$H NMR (500 MHz, $CD_2Cl_2$): $\delta$ 8.18 (d, $J$ = 7.7 Hz, 1H), 7.68 (d, $J$ = 7.3 Hz, 1H), 7.61 (d, $J$ = 8.3 Hz, 1H), 7.35−7.22 (m, 2H), 7.09−7.02 (m, 3H), 6.84 (dd, $J$ = 8.3, 2.3 Hz, 1H), 4.09 (d, $J$ = 5.7 Hz, 1H), 3.53 (s, 3H), 2.92 (dd, $J$ = 15.1, 5.5 Hz, 1H), 2.76 (d, $J$ = 15.1 Hz, 1H), 2.22 (s, 6H), 0.77 (s, 9H). $^{13}$C NMR (125 MHz, $CD_2Cl_2$): $\delta$ 159.6, 152.2, 146.2, 142.5, 140.8, 140.0, 139.6, 133.1, 132.8, 131.1, 130.9, 130.5, 128.2, 127.3, 125.5, 125.2, 119.8, 119.0, 114.0, 109.1, 58.6, 55.4, 35.8, 35.4, 29.0, 20.7, 18.2. Data for *E*-**17**: $^1$H NMR (500 MHz, $CD_2Cl_2$): $\delta$ 7.78 (d, $J$ = 1.9 Hz, 1H), 7.68 (d, $J$ = 8.3 Hz, 1H), 7.63 (d, $J$ = 7.6 Hz, 1H), 7.38 (d, $J$ = 8.0 Hz, 1H), 7.23 (t, $J$ = 7.4 Hz, 1H), 7.08 (d, $J$ = 7.7 Hz, 1H), 7.05−6.97 (m, 2H), 6.93 (dd, $J$ = 8.3, 2.0 Hz, 1H), 4.16 (d, $J$ = 5.7 Hz, 1H), 3.92 (s, 3H), 3.01 (dd, $J$ = 14.9, 5.5 Hz, 1H), 2.84 (d, $J$ = 15.0 Hz, 1H), 2.30 (s, 3H), 2.25 (s, 3H), 0.86 (s, 9H). $^{13}$C NMR (125 MHz, $CD_2Cl_2$): $\delta$ 159.2, 152.5, 146.2, 142.5, 141.2, 139.6, 138.3, 133.9, 133.3, 130.9 (2C), 130.4, 128.5, 127.5, 125.8, 123.9, 120.3, 118.4, 113.3, 111.3, 58.7, 56.0, 35.7, 35.5, 29.1, 20.6, 18.2.

**Computational Chemistry.** The Gaussian 09 program[37] was used for geometry optimizations and the calculation of energies. Geometry optimizations were performed at the B3LYP/6-31G(d,p) level using tight convergence criteria and vibrational analyses of minima and transition states were obtained; minima had no imaginary frequencies, while the transition state was first-order. The reported energies were corrected for Gibbs free energy.

## ■ ASSOCIATED CONTENT

### Supporting Information

NMR spectra of new compounds, kinetic data for motor **7** obtained by means of transient absorption, and computational details. This material is available free of charge via the Internet at http://pubs.acs.org.

## ■ AUTHOR INFORMATION

### Corresponding Author

*E-mail: b.l.feringa@rug.nl.

### Notes

The authors declare no competing financial interest.

## ■ ACKNOWLEDGMENTS

Arjen Cnossen and Jort Robertus are both gratefully acknowledged for their syntheses of **15** and **18** used in the preparation of molecular motors **7** and **17**.

The authors thank the European Research Council (Advanced Investigator Grant 227897; A.C., B.L.F.) and the Ministry of Education, Culture and Science (Gravity Program 024.001.035) for financial support.

## ■ REFERENCES

(1) *Molecular Motors*; Schliwa, M., Ed.; Wiley-VCH: Weinheim, Germany, 2003.
(2) Browne, W. R.; Feringa, B. L. *Nat. Nanotechnol.* **2006**, *1*, 25−35.
(3) Kay, E. R.; Leigh, D. A.; Zerbetto, F. *Angew. Chem., Int. Ed.* **2007**, *46*, 72−191.
(4) Coskun, A.; Banaszak, M.; Astumian, R. D.; Stoddart, J. F.; Grzybowski, B. A. *Chem. Soc. Rev.* **2012**, *41*, 19−30.
(5) Feringa, B. L. *J. Org. Chem.* **2007**, *72*, 6635−6652.
(6) *Molecular Machines*; Kelly, T. R., Ed.; Topics in Current Chemistry, Vol. *262*; Springer: Berlin, 2005.
(7) Credi, A. *Aust. J. Chem.* **2006**, *59*, 157−169.
(8) Balzani, V.; Credi, A.; Venturi, M. *Molecular Devices and Machines—A Journey into the Nano World*; Wiley-VCH: Weinheim, Germany, 2003.
(9) Braunschweig, A. B.; Northrop, B. H.; Stoddart, J. F. *J. Mater. Chem.* **2006**, *16*, 32−44.
(10) Stoddart, J. F. *Acc. Chem. Res.* **2001**, *34*, 410−411.
(11) *Molecular Switches*, 2nd ed.; Feringa, B. L., Browne, W. R., Eds.; Wiley-VCH: Weinheim, Germany, 2011.
(12) *Molecular Machines and Motors*; Sauvage, J.-P., Ed.; Structure and Bonding, Vol. *99*; Springer: Berlin, 2001.
(13) Kelly, T. R. *Acc. Chem. Res.* **2001**, *34*, 514−522.
(14) Tierney, H. L.; Murphy, C. J.; Jewell, A. D.; Baber, A. E.; Iski, E. V.; Khodaverdian, H. Y.; McGuire, A. F.; Klebanov, N.; Sykes, E. C. H. *Nat. Nanotechnol.* **2011**, *6*, 625−629.
(15) Seldenthuis, J. S.; Prins, F.; Thijssen, J. M.; van der Zant, H. S. J. *ACS Nano* **2010**, *4*, 6681−6686.
(16) Liu, Y.; Flood, A. H.; Bonvallet, P. A.; Vignon, S. A.; Northrop, B. H.; Tseng, H.-R.; Jeppesen, J. O.; Huang, T. J.; Brough, B.; Baller, M.; Magonov, S.; Solares, S. D.; Goddard, W. A.; Ho, C.-M.; Stoddart, J. F. *J. Am. Chem. Soc.* **2005**, *127*, 9745−9759.
(17) Eelkema, R.; Pollard, M. M.; Vicario, J.; Katsonis, N.; Ramon, B. S.; Bastiaansen, C. W. M.; Broer, D. J.; Feringa, B. L. *Nature* **2006**, *440*, 163.
(18) Kudernac, T.; Ruangsupapichat, N.; Parschau, M.; Maciá, B.; Katsonis, N.; Harutyunyan, S. R.; Ernst, K.-H.; Feringa, B. L. *Nature* **2011**, *479*, 208−211.
(19) Koumura, N.; Geertsema, E. M.; Meetsma, A.; Feringa, B. L. *J. Am. Chem. Soc.* **2000**, *122*, 12005−12006.
(20) Pollard, M. M.; Klok, M.; Pijper, D.; Feringa, B. L. *Adv. Funct. Mater.* **2007**, *17*, 718−729.
(21) Geertsema, E. M.; van der Molen, S. J.; Martens, M.; Feringa, B. L. *Proc. Natl. Acad. Sci. U.S.A.* **2009**, *106*, 16919−16924.
(22) Pollard, M. M.; Wesenhagen, P. V.; Pijper, D.; Feringa, B. L. *Org. Biomol. Chem.* **2008**, *5*, 1605−1612.
(23) Cnossen, A.; Hou, L.; Pollard, M. M.; Wesenhagen, P. V.; Browne, W. R.; Feringa, B. L. *J. Am. Chem. Soc.* **2012**, *134*, 17613−17619.
(24) Goldstein, H.; Poole, C.; Safko, J. *Classical Mechanics*, 3rd ed.; Addison-Wesley: San Francisco, 2001.
(25) Klok, M. Motors for Use in Molecular Nanotechnology. Ph.D. Thesis, University of Groningen, Groningen, The Netherlands, 2009.
(26) Koumura, N.; Geertsema, E. M.; van Gelder, M. B.; Meetsma, A.; Feringa, B. L. *J. Am. Chem. Soc.* **2002**, *124*, 5037−5051.
(27) Pollard, M. M.; Meetsma, A.; Feringa, B. L. *Org. Biomol. Chem.* **2008**, *6*, 507−512.
(28) Fernández Landaluce, T.; London, G.; Pollard, M. M.; Rudolf, P.; Feringa, B. L. *J. Org. Chem.* **2010**, *75*, 5323−5325.
(29) Vicario, J.; Walko, M.; Meetsma, A.; Feringa, B. L. *J. Am. Chem. Soc.* **2006**, *128*, 5127−5135.
(30) Hart, R. T.; Tebbe, R. F. *J. Am. Chem. Soc.* **1950**, *72*, 3286−3287.
(31) Huang, Y.-S.; Liu, J.-Q.; Zhang, L.-J.; Lu, H.-L. *Ind. Eng. Chem. Res.* **2012**, *51*, 1105−1109.
(32) Garner, P.; Şeşenoğlu, Ö. *Org. Lett.* **2004**, *6*, 1217−1219.
(33) *Synthesis: Carbon with One Heteroatom Attached by a Multiple Bond*; Pattenden, G., Vol. Ed.; Comprehensive Organic Functional Group Transformations, 1st ed., Vol. *3*; Katritzky, A. R., Meth-Cohn, O., Rees, C. W., Series Eds.; Elsevier Science: Cambridge, UK, 1995; p 330−375.
(34) Conyard, J.; Addison, K.; Heisler, I. A.; Cnossen, A.; Browne, W. R.; Feringa, B. L.; Meech, S. R. *Nat. Chem.* **2012**, *4*, 547−551.
(35) Klok, M.; Boyle, N.; Pryce, M. T.; Meetsma, A.; Browne, W. R.; Feringa, B. L. *J. Am. Chem. Soc.* **2008**, *130*, 10484−10485.

(36) Fischer, E. *J. Phys. Chem.* **1967**, *71*, 3704−3706.
(37) Frisch, M. J.; Trucks, G. W.; Schlegel, H. B.; Scuseria, G. E.; Robb, M. A.; Cheeseman, J. R.; Scalmani, G.; Barone, V.; Mennucci, B.; Petersson, G. A.; Nakatsuji, H.; Caricato, M.; Li, X.; Hratchian, H. P.; Izmaylov, A. F.; Bloino, J.; Zheng, G.; Sonnenberg, J. L.; Hada, M.; Ehara, M.; Toyota, K.; Fukuda, R.; Hasegawa, J.; Ishida, M.; Nakajima, T.; Honda, Y.; Kitao, O.; Nakai, H.; Vreven, T.; Montgomery, J. A., Jr.; Peralta, J. E.; Ogliaro, F.; Bearpark, M.; Heyd, J. J.; Brothers, E.; Kudin, K. N.; Staroverov, V. N.; Kobayashi, R.; Normand, J.; Raghavachari, K.; Rendell, A.; Burant, J. C.; Iyengar, S. S.; Tomasi, J.; Cossi, M.; Rega, N.; Millam, J. M.; Klene, M.; Knox, J. E.; Cross, J. B.; Bakken, V.; Adamo, C.; Jaramillo, J.; Gomperts, R.; Stratmann, R. E.; Yazyev, O.; Austin, A. J.; Cammi, R.; Pomelli, C.; Ochterski, J. W.; Martin, R. L.; Morokuma, K.; Zakrzewski, V. G.; Voth, G. A.; Salvador, P.; Dannenberg, J. J.; Dapprich, S.; Daniels, A. D.; Farkas, Ö.; Foresman, J. B.; Ortiz, J. V.; Cioslowski, J.; Fox, D. J. *Gaussian 09*, revision C.01; Gaussian, Inc.: Wallingford, CT, 2009.